AGU ADVANCING EARTH AND SPACE SCIENCE

Earth and Space Science

RESEARCH ARTICLE
10.1029/2019EA001063

Key Points:
- Solar cycle modulation of nighttime ozone is shown with MLS observation near the mesopause
- The semi-annual and solar cycle variations of nighttime ozone is similar to those of nighttime ozone in the mesosphere
- The nighttime ozone variation in the upper mesosphere and lower thermosphere (UMLT) is largely driven by dynamics via Eddy diffusion

Supporting Information:
- Supporting Information S1

Correspondence to:
J. N. Lee,
jae.n.lee@nasa.gov

Citation:
Lee, J. N., & Wu, D. L. (2020). Solar cycle modulation of nighttime ozone near the mesopause as observed by MLS. *Earth and Space Science*, *6*. https://doi.org/10.1029/2019EA001063

Received 19 DEC 2019
Accepted 15 MAR 2020
Accepted article online 20 MAR 2020

Solar Cycle Modulation of Nighttime Ozone Near the Mesopause as Observed by MLS

Jae N. Lee[1,2] and **Dong L. Wu**[2]

[1]Joint Center for Earth Systems Technology, University of Maryland, Baltimore, MD, USA, [2]NASA Goddard Space Flight Center, Greenbelt, MD, USA

Abstract Eleven-year solar cycle variations of nighttime ozone near the secondary ozone maximum layer in the mesosphere are analyzed with Aura Microwave Limb Sounder (MLS) observations since 2004, fully covering solar cycle 24. Produced primarily from the recombination of molecular oxygen (O_2) with atomic oxygen (O) transported from the lower thermosphere, the mesospheric nighttime ozone concentration is proportional to atomic oxygen density [O], which itself is modulated by ultraviolet (UV) solar cycle variations. MLS nighttime ozone data and UV data at 240 nm from Solar Radiation and Climate Experiment (SORCE) Solar-Stellar Irradiance Comparison Experiment (SOLSTICE) show a positive correlation over the solar cycle. Nighttime O_3 and nighttime carbon monoxide (CO) distributions are highly correlated with each other with similar seasonal and solar cycle variations, because both [O_3] and [CO] depend strongly on UV photolysis and are modulated by Eddy diffusion in this region. Nighttime ozone correlates strongly with temperature, with a generally positive correlation, except at high latitudes during boreal winter.

1. Introduction

The presence of an abundant ozone layer in the upper mesosphere and lower thermosphere (UMLT) is known as the secondary ozone maximum, next to the maximum ozone layer in the stratosphere (Smith & Marsh, 2005, and references therein). While extensive studies have been carried out to search for evidence of interannual variation of stratospheric O_3 associated with the 11-year solar cycle, both from observations and models (Aquila et al., 2016; Ball et al., 2019; Li et al., 2016; Maycock et al., 2016, 2018; Merkel et al., 2011; Swartz et al., 2012), the secondary ozone maximum layer has been less explored than the stratospheric ozone.

While the radiation, dynamics, and chemistry in the UMLT are largely driven by solar radiation, solar cycle-driven UV irradiance changes are expected to significantly modulate ozone abundances within the secondary ozone maximum layer. Substantial variation in solar UV irradiance, larger than several percent over the 11-year solar cycle (Lee et al., 2016), directly impacts ozone chemistry, because the major single source of secondary maximum ozone production is photochemistry of oxygen species from the Chapman cycle (Chapman, 1930). This ozone production photochemistry involves reaction between atomic oxygen (O) and molecular oxygen (O_2),

$$O_2 + h\nu \rightarrow O + O, \quad \text{(R0)}$$

$$O + O_2 + M \rightarrow O_3 + M, \quad \text{(R1)}$$

where M indicates the total density of the atmosphere.

The major photochemical reactions for ozone destruction are:

$$O_3 + h\nu \rightarrow O + O_2 \quad \text{(R2)}$$

$$O_3 + O \rightarrow 2O_2 \quad \text{(R3)}$$

$$O_3 + H \rightarrow OH + O_2 \quad \text{(R4)}$$

Photolysis of ozone [(R2)] from solar irradiance in the Schumann-Runge bands (176–192.6 nm) and Herzberg continuum (200–240 nm) is known as the largest ozone loss mechanism in the secondary ozone

maximum region (Smith & Marsh, 2005). Ozone is mostly destroyed via photolysis by solar radiation [(R2)] into atomic oxygen [O] and molecular oxygen [O_2], but these oxygen species also produce ozone through the recombination process [(R1)]. During the day, reaction [(R2)] dominates the loss process and the ozone concentration under chemical equilibrium is determined by

$$[O_3] = \frac{k_1[O][O_2][M]}{J_2 + k_3[O] + k_4[H]}, \tag{1}$$

where the k_1 values represent rate coefficients for reactions [(R1)]. Daytime ozone has a very short lifetime because the J_2 loss term is much larger than the k_3 and k_4 loss terms. During nighttime, when [(R2)] is absent, reactions with atomic oxygen [(R3)] and atomic hydrogen [(R4)] are the only significant sinks for ozone in the mesosphere. As shown in Smith and Marsh (2005), [(R3)] is a slow reaction, and the nighttime ozone loss is dominated by [(R4)]. Recent study has shown that the reaction of O + O_3 also plays an important role in O_3 loss process near the mesopause (Zhu & Kaufmann, 2018). A similar assessment was found by Allen et al. (1984), showing in the upper mesosphere above ~80 km the nighttime ozone is largely balanced by reactions [(R1)] and [(R4)]. Hence, in chemical equilibrium, to first order, the UMLT nighttime ozone abundance can be deduced from

$$[O_3] = \frac{k_1[O][O_2][M]}{k_4[H]}. \tag{2}$$

Thus, the amount of nighttime ozone under chemical equilibrium is not only proportional to [O] and [O_2] but also inversely proportional to atomic hydrogen density [H]. Under chemical equilibrium, primarily through the temperature dependence of reaction [(R1)], an anticorrelation between ozone and temperature is expected (Brasseur & Solomon, 2005), if [H], [O], and [O_2] are kept constant.

It is important to put the odd oxygen chemistry into perspective of the UMLT dynamics as the photochemical lifetimes are competing with the dynamical lifetimes associated with these species (Garcia & Solomon, 1985). The chemical lifetime of odd oxygen increases from 10^4 s in the upper mesosphere to 10^8 s in the lower thermosphere, whereas the dynamical time scale of the eddy diffusion coefficient (k_{zz}) is generally ~10^6 s. This leads to a transition from chemical to dynamical control in terms of odd oxygen variability with a crossover at ~85 km. Under chemical control, as expressed by equation (2), nighttime ozone variability is proportional to the [O]/[H] ratio through a balance between reactions [(R1)] and [(R4)]. Using the nighttime atomic hydrogen and atomic oxygen densities inferred from Solar Mesosphere Explore (SME), Thomas (1990) showed that tropical [O] and [H] at 0.003 hPa have a strong semiannual oscillation (SAO) with higher [O] and lower [H] volume mixing ratios (VMRs) at the equinox, which is consistent with the SAO of ozone derived from SME OH airglow measurements.

Garcia and Solomon (1985) emphasized the role of eddy diffusion in modulating odd oxygen variability in the UMLT region. With weaker diffusion/mixing (lower k_{zz}) in the UMLT, odd oxygen resides longer in the lower thermosphere, allowing it more time to accumulate. In the case of stronger diffusion/mixing, more odd oxygen is subject to chemical loss at a lower altitude, leading to a lower concentration in the UMLT. The coupled dynamical and chemical influences are able to explain the SAO variations seen in [O] and [O_3], as the UMLT k_{zz} is generally smaller near the equinox. Such dynamics-chemistry coupling has been further explored in recent studies (e.g., Dikty et al., 2010; Garcia et al., 2014; Smith & Marsh, 2005; Tweedy et al., 2013).

In addition, ionization by energetic particle precipitation, primarily by high-energy electrons with energies greater than 100 keV in the auroral regions, is suggested as another short-term mesospheric ozone depletion mechanism (Andersson et al., 2014; Turunen et al., 2016). By enhancing the HO_x and NO_x productions, large solar photon events can also induce significant ozone loss in the UMLT (Jackman et al., 2008, 2011).

Diurnal variations of mesospheric ozone have been explored by Marsh et al. (2002), using day-night differences observed by the high resolution Doppler imager and by Dikty et al. (2010), using daytime measurements from Sounding of the Atmosphere using Broadband Emission Radiometry (SABER). The mesospheric ozone climatology and diurnal differences between nine satellite data sets have been documented in great detail by Smith et al. (2013). It was pointed out that potential sampling biases from different

ozone observations and models could result in improper diurnal variation of mesospheric ozone (Studer et al., 2014).

There is a positive ozone response to the 27-day solar rotational variation from a number of studies (Gruzdev et al., 2009; Hood & Zhou, 1998; Ruzmaikin et al., 2007; Thiéblemont et al., 2018). The 11-year solar cycle response of ozone in the middle atmosphere has been also explored by many authors (e.g., Crooks & Gray, 2005; Dhomse et al., 2016; Haigh et al., 2010; Hood et al., 1991; Huang et al., 2008; Soukharev & Hood, 2006; Tang et al., 2018). Despite many efforts to explore different data sets and analysis methods, the amplitude of variations associated with the solar cycle and the response mechanism of mesospheric ozone to UV variation are still not well characterized. In the lower mesosphere, the observed ozone responses to solar forcing from previous works do not agree in magnitude nor in phase with respect to the solar cycle (Beig et al., 2012; Merkel et al., 2011).

Characterizing solar cycle ozone variations and their coupling with atmospheric chemistry and dynamics has been a challenge because ozone measurements inferred from photochemical reactions are often prone to errors in other photochemically active species used in the ozone retrievals. Scarcity of reliable long-term observations and lack of independent validation of ozone data in the upper atmosphere have led to many controversial views on ozone variability.

Long-term observations from two satellite instruments, SOlar Radiation and Climate Experiment (SORCE, 2003–present) and Microwave Limb Sounder (MLS, 2004–present) on Aura, now enable us to examine the direct and indirect responses of ozone in the UMLT region to 11-year solar cycle variability. MLS operates with a regular limb scan up to ~90 km, observing directly through the secondary ozone peak in the upper atmosphere. While the profile from individual scans is noisy, MLS daily mean radiances are quite sensitive to small ozone changes in the mesopause region. In this paper, we discuss nighttime variations of MLS ozone and their relationships to 11-year UV variations at the lower end (i.e., 0.002 hPa) of the secondary ozone maximum layer.

2. Data

2.1. Microwave Limb Sounder (MLS)

We use MLS version 4.2× (V4.2×) data (Froidevaux et al., 2008) for daily nighttime ozone, at the 0.002 hPa level. We refer the nighttime ozone as MLS observations for solar zenith angles larger than 90° from either ascending or descending orbits. The ascending nodes of the orbit (i.e., when the spacecraft is moving toward the north) cross the equator at 1:45 ± 15 p.m. local time, and the descending nodes of the orbit (i.e., when the spacecraft is moving toward the south) cross the equator at 1:45 ± 15 a.m. Since the orbital period of the Aura spacecraft is approximately 100 min, the local time of MLS observation changes within ±25 min from the ascending or descending nodes depending on latitudes (https://aura.gsfc.nasa.gov/scinst.html).

The ozone data are aggregated into 43 latitude bins between 82°N and 82°S, because Aura MLS sampling does not cover the regions poleward of 82°N/°S latitude. The vertical resolution of O_3 is from 5 to 7 km over the 0.01 to 0.001 hPa domain. The recommended topmost pressure level for the ozone for scientific use is 0.02 hPa (https://mls.jpl.nasa.gov/data/v4-2_data_quality_document.pdf). The 2σ estimate of systematic uncertainty is ~0.2 ppmv or 50% at 0.02 hPa. Although the recommended pressure level for ozone studies is 0.02 hPa, there is still some MLS sensitivity in the uppermost mesosphere (Froidevaux et al., 2008). The levels up to 0.002 hPa contain valuable information on mesospheric ozone (Livesey and Froidevaux, 2019, private communication). The MLS ozone data at this level have been studied previously by Andersson et al. (2014) and Hocke (2017), showing that they are scientifically useful even above the validated single-profile height levels.

The MLS mesospheric ozone is retrieved from an emission feature at 235.71 GHz. As shown in Figure 1, MLS resolves this emission line spectrally with a 25-channel filter bank with variable bandwidths between 6 and 96 MHz. In the mesosphere, the O_3 emission mostly resides in the 6-MHz center channel (Channel 13), while the radiances from Channels 1–3 and 23–25 can be used to estimate the background from calibration residuals or other variations that may change with time and orbit. The difference between Channel 13 and the background radiances constitutes the mesospheric O_3 radiance signal, which contributes the most to MLS mesospheric ozone VMR retrievals. The daytime radiance (not shown) is nearly zero at upper

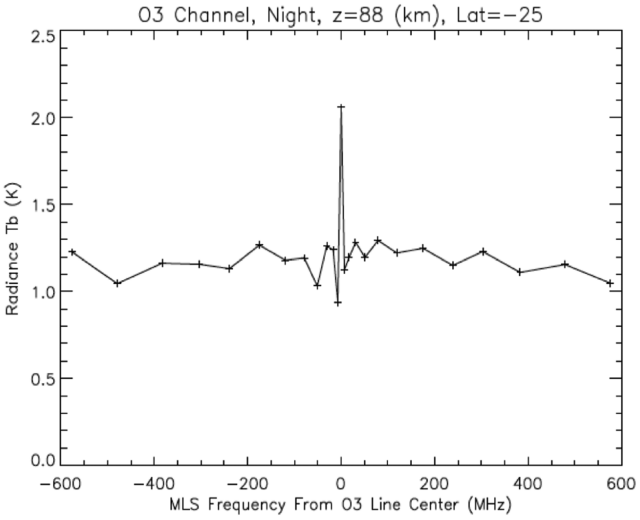

Figure 1. MLS brightness temperature (T_b) from the ozone channel centered at 235.71 GHz. The center channel of the MLS 25-channel filter bank has 6-MHz bandwidth and shows a significant ozone signal above the background.

mesospheric heights. Since the nighttime O_3 emission near the mesopause is very weak, a careful removal of the instrument background radiance is critical to observe weak solar cycle variations.

To further evaluate the MLS sensitivity to mesospheric nighttime ozone abundance and its variation with respect to the solar cycle, we average three 96-MHz wing channels (Channels 1–3 and 23–25) at tangent heights above 80 km and subtract this signal from the Channel 13 radiances to obtain the background radiances at about 88 km.

Figure 2 shows a time series of the extracted nighttime ozone radiances at 88 km for 2004–2019. The daily ozone radiances show strong annual and semiannual variations at 88 km around the equator. The solar cycle amplitude is obtained from the 11-year period fit after the seasonal cycle is removed. In this case, the regressed 11-year peak-to-peak amplitude is 90 mK with an uncertainty of 5.9 mK. This clear solar cycle signal in radiances agrees very well with variations in MLS retrieved ozone at 0.002 hPa, providing further confidence in the results of mesospheric ozone analyses presented later in this paper.

The residual of the fit is ±0.4 K and is mostly from the measurement noise. There may be some contributions from atmospheric variability that is not seasonal. The MLS Level 2 algorithm employs the subtraction of a varying background from the wing channels (Froidevaux et al., 2008). Therefore, the measurement uncertainty is a combined error from the center channel radiance and the estimated background radiance.

MLS mesospheric ozone data can be valuable especially for long-term ozone variation studies. The MLS standard O_3 product acquired from 235.71 GHz radiances shows no significant temporal drift, in comparison to other ground-based measurements (Hubert et al., 2016).

We have also analyzed MLS mesospheric carbon monoxide (CO) and temperature (T) data (Livesey et al., 2017), since mesospheric CO is a good dynamics tracer due to its long lifetime. The typical single-profile precision of MLS V4.2× CO varies from 0.02 ppmv at 100 hPa to 0.2 ppmv at 1 hPa, and 11 ppmv at 0.002 hPa, with vertical resolution of 4, 3, and 9 km, respectively. MLS temperature in the mesosphere is retrieved primarily from bands near O_2 spectral lines at 118 GHz. The precision of the MLS V4.2× temperature measurement is ±3.6 K, and the bias is ~3 K between 0.01 and 0.001 hPa. In the mesosphere between 0.01 and 0.001 hPa, the MLS temperature profiles have a vertical resolution of 8–13 km, a precision of 2.2–2.5 K, and a 4–8 K cold bias.

2.2. SORCE SOLSTICE

The SOlar-Stellar Irradiance Comparison Experiment (SOLSTICE) on SORCE measures ultraviolet (UV) solar irradiances from 115 to 320 nm with a resolution of 0.1 nm, an absolute accuracy of better than 5%, and a relative accuracy of 0.5% per year (McClintock et al., 2005; McClintock et al., 2005; Snow et al., 2005). The SOLSTICE measurements are made of a pair of identical spectrometers, SOLSTICE A and SOLSTICE B. Each instrument independently measures ultraviolet solar irradiance in two intervals: far ultraviolet at 115–180 nm and mid-ultraviolet at 180–320 nm.

3. Results

3.1. Nighttime Ozone Climatology

The vertical profile of ozone VMR in the UMLT is shown for the tropics in Figure 3. The MLS nighttime ozone exhibits a secondary peak near the mesopause (~0.001 hPa). At the tropics, the secondary maximum amount of nighttime ozone is ~6 ppmv, and this amount is comparable to ~60% of the ozone amount at the stratospheric maximum (~10 ppmv). Daytime ozone VMR is substantially smaller than nighttime ozone in this region but is significantly higher than that in the middle and lower mesosphere.

The 15+ years of Aura MLS ozone and CO observations provide new insights on the interannual variation of ozone associated with chemistry and dynamics in the middle atmosphere. There is a strong correlation

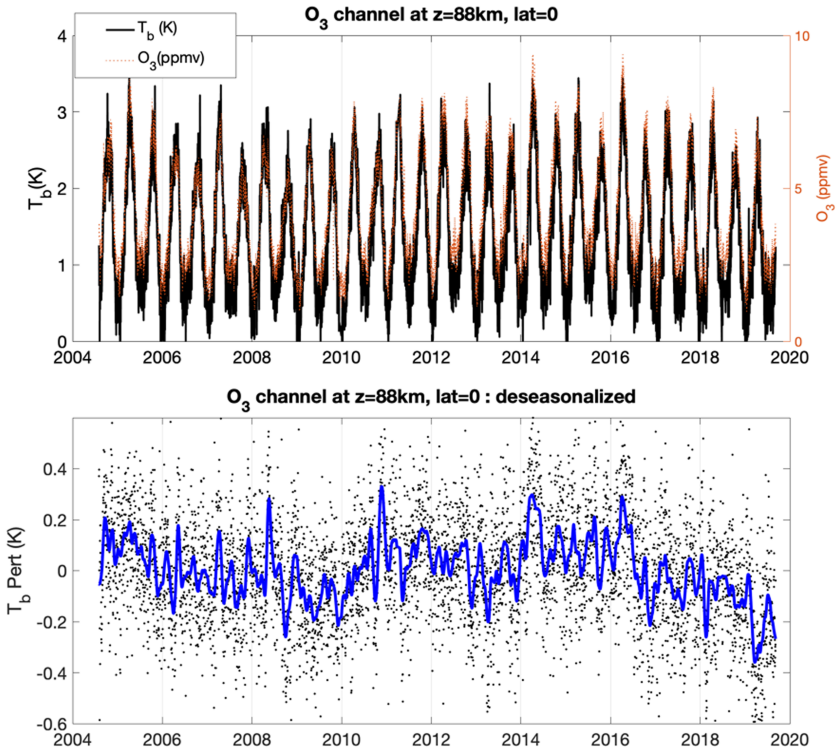

Figure 2. Time series of MLS 235.71-GHz radiances at 88 km at the equator (2.5°S–2.5°N). The top panel is the nighttime radiance with the background radiance removed, whereas the bottom panel is the de-seasonalized series to highlight the 11-year variation with superimposed a 50-day running smooth curve.

between MLS O_3 and CO in the upper mesosphere (see more discussion later). To illustrate the seasonal variations of the ozone distribution, the climatology of nighttime mesospheric ozone VMR during the MLS observation period (2004–2019) is shown in Figure 4. The figure shows MLS nighttime ozone climatology at 0.002 hPa pressure level in different latitude bands. Even though the MLS observations cannot give a full coverage of the secondary maximum ozone layer in the UMLT above 0.001 hPa, MLS ozone clearly shows the lower part of the maximum layer in the upper mesosphere. The ozone VMR at 0.002 hPa reaches up to 6 ppmv in high latitudes and up to 7 ppmv near the tropics at this level. However, the plot also shows low amount of ozone (below 2 ppmv) during the local summer season.

In the high-latitude (60°N/°S–82°N/°S) regions, MLS nighttime ozone VMR shows a large annual cycle superimposed on a semiannual cycle, with an early winter maximum and an early summer minimum. The ozone climatology also displays hemispheric differences between SH (Southern Hemisphere) and NH (Northern Hemisphere), with slightly more ozone in the NH than in the SH during the early winter maxima. In each case, the MLS nighttime ozone climatology shows a semiannual oscillation (SAO) with two seasonal maxima, in early winter (October/November in NH and April/May in SH) and in early spring (February/March in NH and August/September in SH). The peak in early winter is slightly higher than that in early spring.

In the tropics, the seasonal variation of nighttime O_3 shows an obvious SAO with two equinoctial peaks during April and October, with a slightly larger peak in April. Similar to those at high latitudes, the SAO seasonal minima during solstice show ~2 ppmv ozone VMR, approximately one third of the equinoctial maximum values. The amplitude of the SAO in the tropics corroborates the monthly O_3 densities estimated from 1D model simulations by Gattinger et al. (2013). Their simulated nighttime O_3 densities and the observed Envisat/GOMOS (Global Ozone Monitoring by Occultation of Stars) O_3 densities are approximately three times larger during the SAO maximum in April, compared to the densities during SAO minimum in August.

Overlaid red curves in Figure 4 denote MLS nighttime CO climatology during the same period. The seasonal variations of nighttime ozone are quite similar to those of CO, indicating similar dynamical and

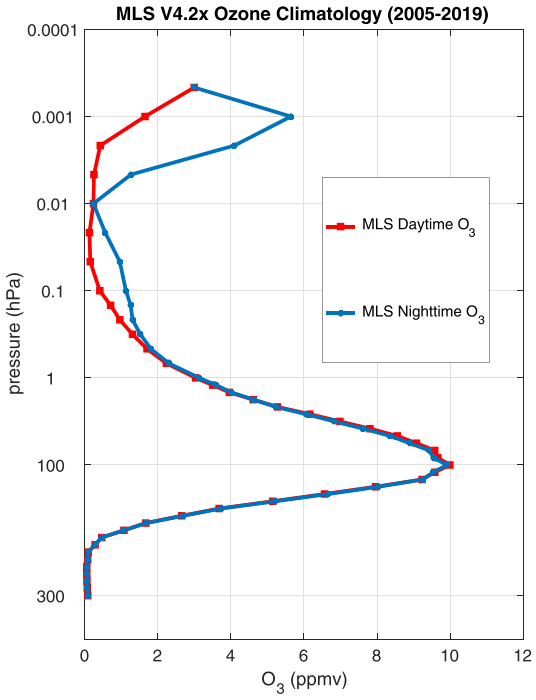

Figure 3. Climatology of vertical profiles of MLS V4.2× nighttime (blue) and daytime (red) O_3 VMRs during 2005–2019 at the equator (4°S–4°N).

photochemical processes associated with atomic oxygen. Details of the CO climatology have been described by Lee et al. (2018).

3.2. Interannual Variation of Nighttime Ozone

MLS nighttime zonal mean ozone VMR time series are shown in Figure 5 for (a) northern high latitudes (60°N–82°N), (b) southern high latitudes (60°S–82°S), and (c) the tropics (12°S–12°N) at 0.002 hPa. The ozone in SH high latitudes (Figure 5b) shows a similar annual cycle as in the NH, but with approximately a 6-month phase shift versus that from the NH, as already shown in Figure 4. The ozone VMR time series shows the SAO cycle in the tropics, with two almost equal maxima.

Besides the annual oscillations, MLS nighttime ozone time series show more than 2 ppmv of interannual variation, with a minimum during 2008–2009, a maximum during 2012–2014, and another minimum during 2018–2019. This is indicative of the 11-year solar cycle modulation, since solar cycle 24 was at solar minimum during 2008–2009, solar maximum during 2014–2015, and is approaching solar minimum again during 2019. Nighttime ozone variation with the 11-year solar cycle will be further discussed in section 3.3.

3.3. Solar Cycle Variation of Nighttime Ozone

MLS O_3 zonal mean anomaly data show a strong interannual variation during the analysis period (2004–2019) that correlates with the 11-year solar cycle. Shown in Figure 6 are interannual variations of high-latitude ozone anomalies during 2 months near the seasonal maximum (November/December for NH and March/April for SH) at 0.002 hPa, overlaid with SORCE/SOLSTICE UV at 240 nm. In the NH high latitudes (Figure 6a), the nighttime ozone anomaly varies by up to 2 ppmv, showing 1 ppmv less than average ozone amounts during the solar minimum period. Similarly, the ozone anomaly variation in the SH high latitudes (Figure 6b) shows an in-phase variation with the 11-year solar cycle within 1.5 ppmv.

Our result, more than 25% of nighttime ozone variation with a solar cycle correlation at this level, corroborates the Hamburg Model of Neutral and Ionized Components (HAMMONIA) simulations by Beig et al. (2012). Their 2D simulation exhibits a strong positive (~40–45%/100 sfu) ozone response to solar forcing near 0.0023 hPa (~90 km) in 40°N/°S–60°N/°S latitude bands. Since the F10.7 radio flux changes ~100 sfu over one solar cycle, their solar cycle variation amplitudes (in %/100 sfu) are comparable to our estimate of solar cycle response of ozone. However, our MLS data analysis level, 0.002 hPa, is close to the top of the retrievals and its averaging kernel shows a substantial (~40%) contribution from the modeled a priori at the top level (Froidevaux et al., 2008) which does not vary with solar cycle. This may cause an underestimation of the actual amplitude of the solar cycle response of the current analysis, although it is difficult to estimate how much uncertainty this effect would add.

In the upper mesosphere (0.001 hPa), there exists an in-phase ozone variation within 3 ppmv (50%) versus the solar cycle. In the lower mesosphere below 0.002 hPa, the zonal mean ozone is less than 2 ppm and decreases by 0.5 ppm at 0.005 hPa when UV is increased (not shown). Even though this small amount of solar cycle variation is difficult to assess from the MLS observations, ozone in the lower mesosphere is expected to be decreased with solar cycle when nighttime ozone increases in the upper mesosphere. Since more UV is absorbed by increased ozone above, less UV is transmitted to the lower mesosphere. Reduced UV leads to less O_2 photolysis, and therefore less O_3 is expected in the lower mesosphere.

3.4. Correlation Between Nighttime Ozone (O_3) and Carbon Monoxide (CO)

CO has a major source from CO_2 photolysis in the UMLT region, that is,

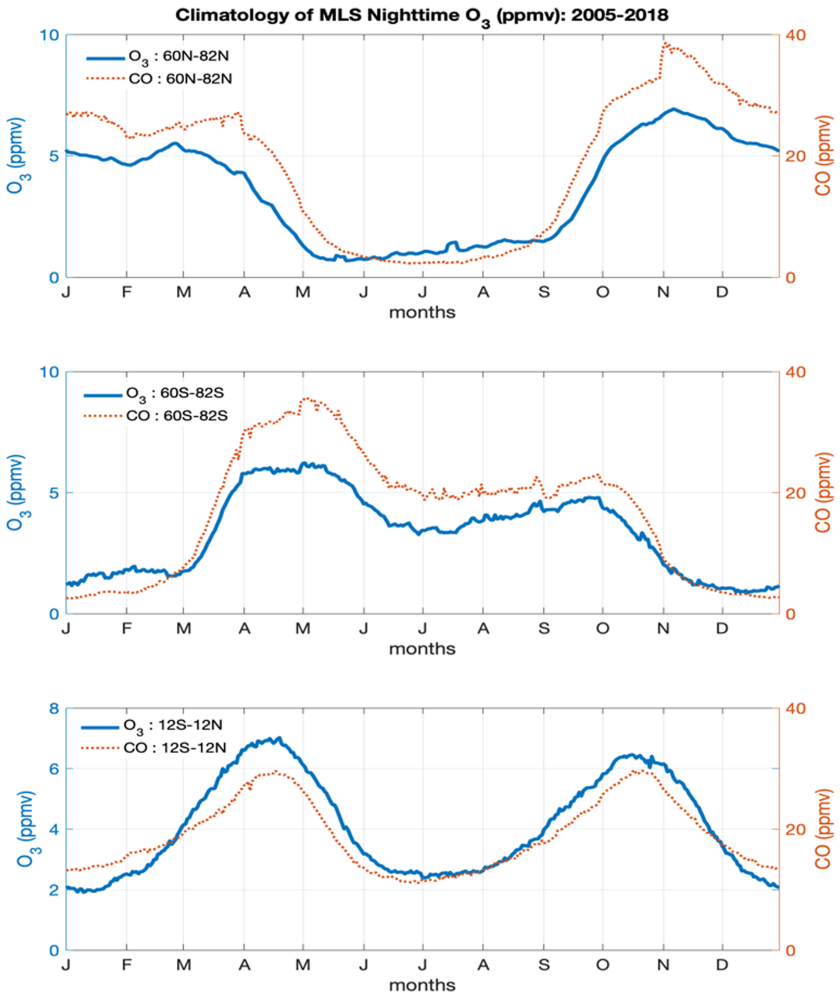

Figure 4. Climatology of MLS nighttime ozone VMR (ppmv) at 0.002 hPa during the MLS observation period (2005–2018) for the NH high latitude (60°N–82°N), SH high latitude (60°S–82°S), and tropics (12°S–12°N), from the top. Overlaid red curves are the same, but for MLS nighttime CO.

$$CO_2 + h\nu \rightarrow CO + O. \tag{R5}$$

In the lower thermosphere, the main loss of CO is through three-body recombination with atomic oxygen, which is a slow reaction:

$$CO + O + M \rightarrow CO_2 + M. \tag{R6}$$

From the mesosphere to stratosphere, a rapid loss process becomes increasingly important through the reaction (Solomon et al., 1985),

$$CO + OH \rightarrow CO_2 + H. \tag{R7}$$

Thus, the CO concentration under chemical equilibrium can be expressed by

$$[CO] = \frac{J\,[CO_2]}{k_6[O][M] + k_7\,[OH]}, \tag{3}$$

where J is the photo-dissociation rate constant for CO_2 [(R5)] and k is the reaction rate constant. In the UMLT the CO concentration is largely a result of photochemical balance between reactions [(R5)] and [(R6)], meaning that the second term in the dominator above becomes negligible.

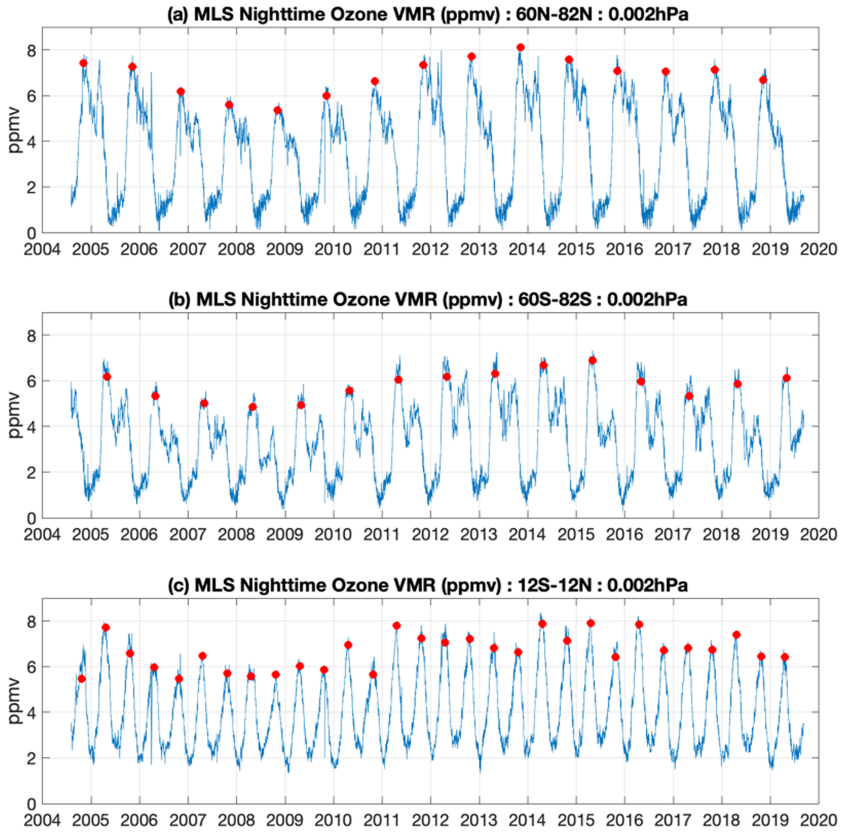

Figure 5. (a) MLS daily zonal mean nighttime O_3 VMR time series at 0.002 hPa (a) in NH high latitude (60°N–82°N), (b) in SH high latitude (60°S–82°S), and (c) in the tropics (12°S–12°N). Red markers in each line plot in (a), (b), and (c) indicate the annual and semiannual maxima of the O_3 mixing ratios.

Like nighttime ozone, CO variability has both dynamical and chemical influences in the upper mesosphere with the crossover height at ~75 km (Solomon et al., 1985), slightly lower than the height of odd oxygen. Therefore, the UMLT CO is largely under dynamical control, which makes it a good dynamical tracer.

Supply of UV provides favorable conditions for CO production with CO building up as the solar radiation increases during solar maximum. CO shows an in-phase relation with the 11-year solar cycle throughout the mesosphere, because the long lifetime of CO in the upper mesosphere allows CO to be transported downward toward the lower mesosphere (Lee et al., 2018; Lee & Wu, 2013).

As shown in Figure 7, the strong correlation between MLS nighttime ozone and CO VMRs for all latitude bins confirms the dynamical modulation of nighttime ozone in the UMLT region. CO and O_3 are highly correlated in the tropics, in particular. The correlation is relatively low during NH late winter, January and February, when an anomalous amount of CO transport from the thermosphere happens during stratospheric sudden warming (SSW) events. CO has a photochemical lifetime longer than 30 days, due to low amounts of OH during the polar night (Minschwaner et al., 2010), which allows it to be transported to the mesosphere through the strong mesospheric polar vortex during the SSW (Lee et al., 2011). Due to very low concentrations of ozone during JJA (June, July, and August) in the NH, the correlation is nearly zero during that time. The regression coefficients and linear correlation coefficients between ozone and CO, for each month, are summarized in Table 1.

Covariance between ozone and CO VMR time series is further shown for the tropics (12°S–12°N) in Figure 8. They show similar strong SAO oscillations and interannual variabilities. It was suggested in the early study by Dunkerton (1982) that the SAO is generated by gravity wave momentum, as waves in the easterly and westerly phases are alternatively propagated through the semiannual variation of wind phases near the stratopause. Many authors proposed detailed mechanisms associated with the SAO for equinox and solstice

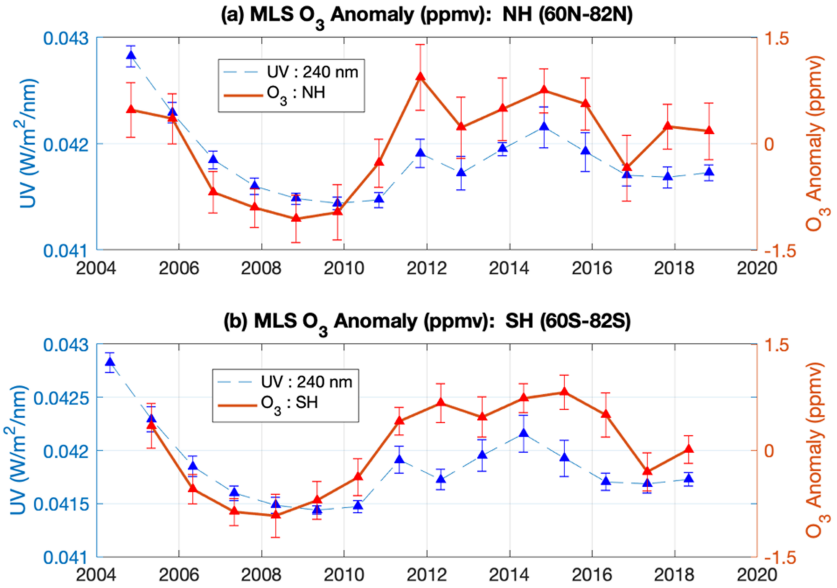

Figure 6. High latitude (a) NH (60°N–82°N) and (b) SH (60°S–82°S) zonal mean MLS O_3 anomaly (in ppmv) during early winter (November/December for NH and March/April for SH) at 0.002 hPa. Overlaid blue curves are SORCE SOLSTICE UV values (in $W/m^2/nm$) at 240 nm to illustrate the UV variation during the same period. The error bars indicate standard deviations of each data calculated from daily values during 2 months of analysis periods.

seasons, but vertical advection and eddy diffusion are commonly accepted as major contributing factors for the SAO generation (Gattinger et al., 2013; Qian et al., 2009, and references therein).

The mechanism of eddy diffusion variations, as suggested by Garcia and Solomon (1985), can explain the SAO in CO. They found that eddy diffusion in the lower thermosphere was maximum in the summer hemisphere and had a significant effect on the seasonal variation of atomic oxygen. The major CO loss in the mesosphere is through reaction with OH. Thus, a stronger k_{zz} in the upper mesosphere will lead to lower [CO] by mixing it down to the chemically lossy mesosphere. The eddy diffusion modulation mechanism can also explain the nighttime ozone variations in this region through its relationship with [O] (see the next section).

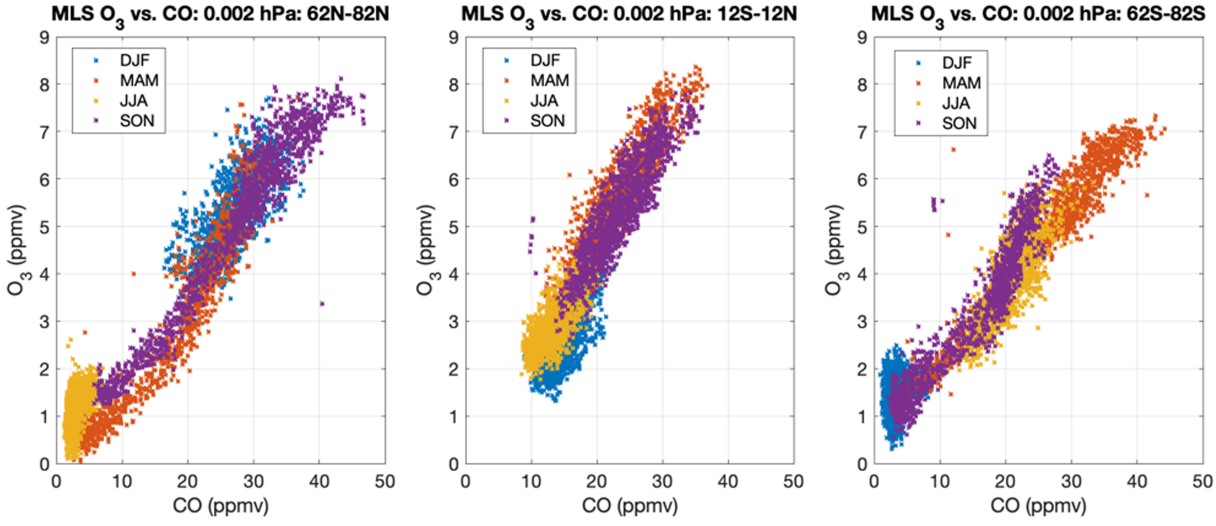

Figure 7. Correlation between MLS daily nighttime ozone and nighttime CO VMRs during 2004–2019 at 0.002 hPa for northern high latitudes (60°N–82°N) (left), tropics (12°S–12°N) (middle), and southern high latitudes (60°S–82°S) (right). Colors denote different seasons as indicated by the legend.

Table 1
Regression Coefficients and Linear Correlation Coefficients Between MLS O_3 and CO for Each Month During 2004–2019

	NH (60°N–82°N)			Tropics (12°S–12°N)			SH (60°S–82°S)		
	a	b	r	a	b	r	a	b	r
January	0.15	0.98	0.73	0.1	0.76	0.53	0.10	1.3	0.15
February	0.19	0.49	0.76	0.18	−0.07	0.58	−0.03	1.9	−0.23
March	0.18	0.33	0.68	0.23	0.31	0.81	0.19	0.26	0.97
April	0.22	−1.4	0.88	0.19	1.3	0.79	0.15	1.2	0.83
May	0.07	0.39	0.57	0.22	0.6	0.89	0.15	0.89	0.88
June	0.00	0.85	0.00	0.13	1.2	0.50	0.18	0.0	0.83
July	0.16	0.73	0.26	0.06	1.8	0.36	0.21	−0.54	0.79
August	0.05	1.3	0.24	0.15	0.88	0.68	0.27	−1.4	0.85
September	0.17	0.1	0.96	0.18	1.1	0.76	0.20	0.39	0.66
October	0.22	−0.78	0.84	0.20	0.56	0.78	0.19	0.10	0.88
November	0.15	1.1	0.81	0.23	0.08	0.87	0.15	0.69	0.66
December	0.18	0.48	0.75	0.18	0.48	0.76	−0.1	1.2	−0.17

Note. The regression coefficients represent $y = ax + b$, when x = CO VMR (ppmv) and $y = O_3$ VMR (ppmv).

As seen in Figure 9, MLS nighttime O_3 and CO at 0.002 hPa show generally consistent latitudinal distributions in each month, except during local winters at mid-to-high latitudes. The monthly distributions track each other in great detail including the equatorial enhancement in the months near the equinox. As discussed in the section 4.2, the nighttime [O_3] could be viewed as an [O] tracer at most latitudes. The modulation of k_{zz} has a similar effect on long-lived species such CO and O, and this is thought to be the key mechanism for the observed latitude distributions, including the tropical enhancement in the equinox months. Because the nighttime [O_3] depends strongly on [O] in the upper mesosphere, it is expected that nighttime [O_3] would follow the [O] distributions in the vicinity of the abundant oxygen number density. The solar cycle variation of [O] is shown from the Scanning Imaging Absorption Spectrometer for Atmospheric Cartography (SCIAMACHY) observations (Zhu et al., 2015). The solar minimum to solar maximum variation from SCIAMACHY [O] is found to be from 10–15% (90 km) to 20–25% (103 km) over the equatorial region (0–20°N).

4. Discussion

4.1. Temperature Dependence of Nighttime Ozone

If the ozone in the secondary maximum layer were under chemical control, its variation would be sensitive to temperature variations and anticorrelation between ozone and temperature is expected (Hood, 1986;

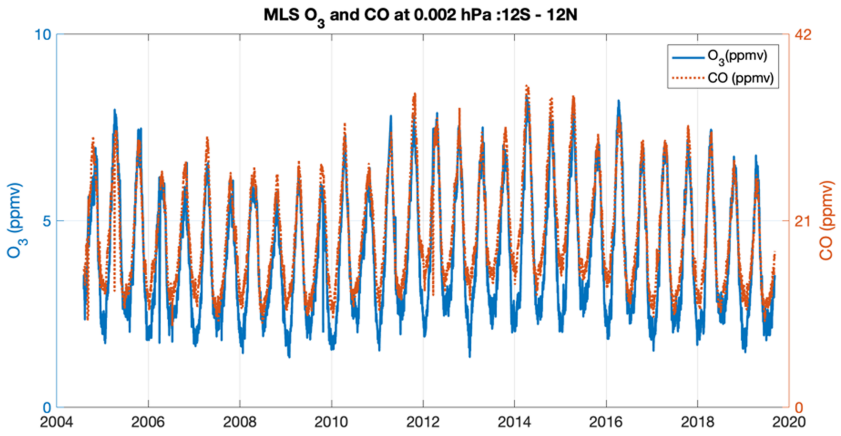

Figure 8. MLS zonal mean nighttime O_3 and CO VMR time series of at 0.002 hPa in the tropics (12°S–12°N). Blue curve in the plot indicates O_3 VMR (in ppmv) and red dots indicate CO VMR (in ppmv).

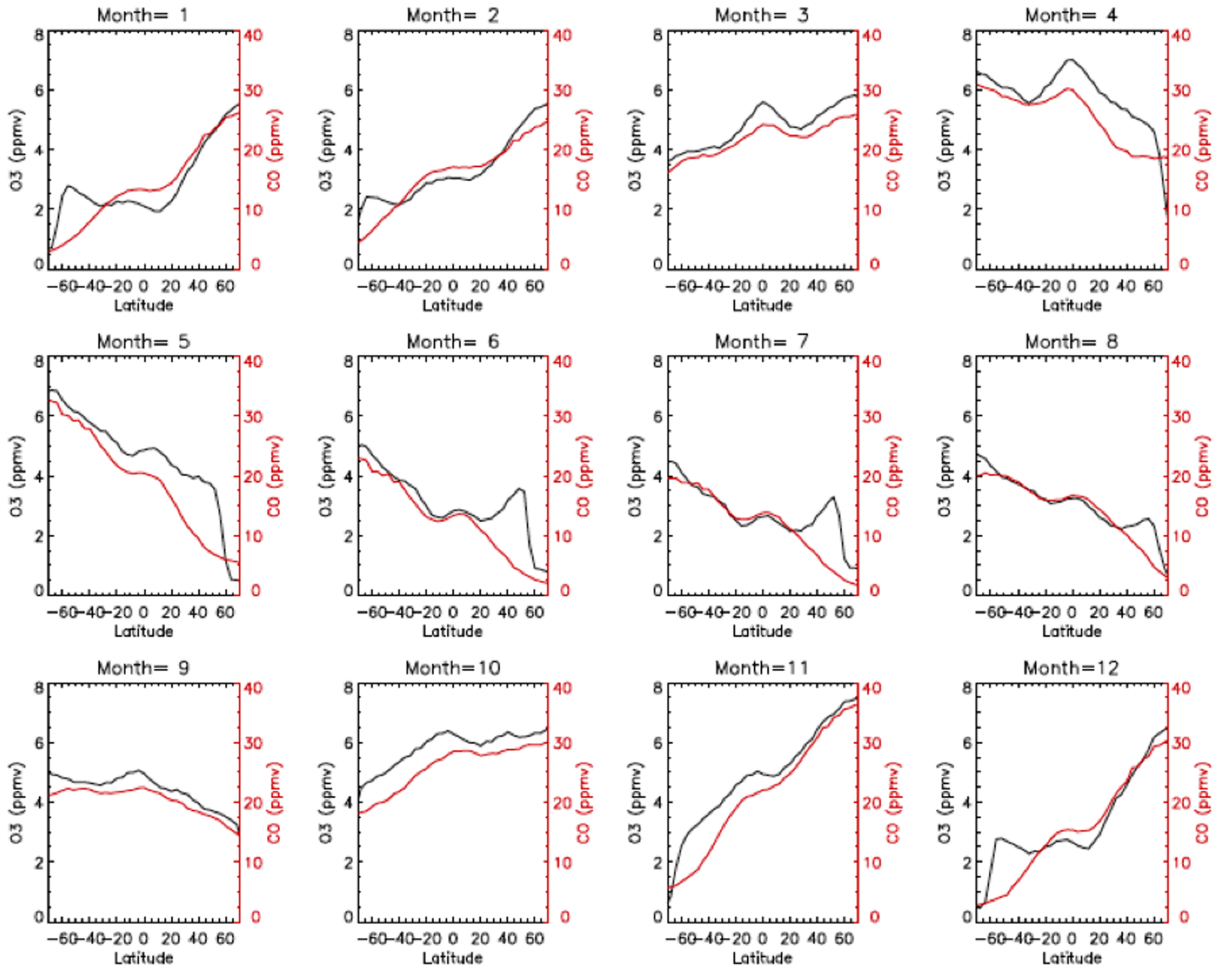

Figure 9. Latitudinal distributions of monthly mean nighttime ozone and CO at 0.002 hPa.

Hood et al., 1991; Smith & Marsh, 2005; Tang et al., 2018). The very low temperatures at the mesopause can accelerate the formation of ozone and suppress the ozone loss. It is also suggested that the nighttime secondary ozone layer is enhanced during SSWs due to adiabatic cooling in the polar mesosphere caused by polar descent (Tweedy et al., 2013).

To examine the temperature dependence of nighttime mesospheric ozone, we correlate the MLS daily nighttime means of ozone mixing ratio and temperature at 0.002 hPa. As shown in Figure 10, the temperature dependence of nighttime ozone is not monotonously positive nor negative but changes with location and season, indicating complex roles of temperature in ozone chemistry and middle atmosphere dynamics. Depending on location and time of the analysis, there is a mixture of positive and negative correlations. Strong positive temperature dependence during fall (SON) is found in all three latitude bins. For other seasons, the overall temperature-ozone correlations are generally positive, except northern high-latitude winter.

The observed positive ozone-temperature correlation is consistent with the expectation that the nighttime near-mesopause ozone is largely under dynamical control (Garcia & Solomon, 1985). The residual meridional circulation near the mesopause, due to gravity wave breaking (e.g., Holton, 1983; Leovy, 1964), leads to descending motions over the winter pole with associated adiabatic heating. This dynamical heating produces higher temperatures in the winter upper mesosphere. Because of the large amount of ozone near the mesopause (i.e., the lower part of the secondary ozone layer), the residual meridional circulation and vertical motions at high latitudes produce higher ozone concentration in the winter hemisphere. On the contrary, ascending motions over the summer pole lead to adiabatic cooling and low temperature anomalies.

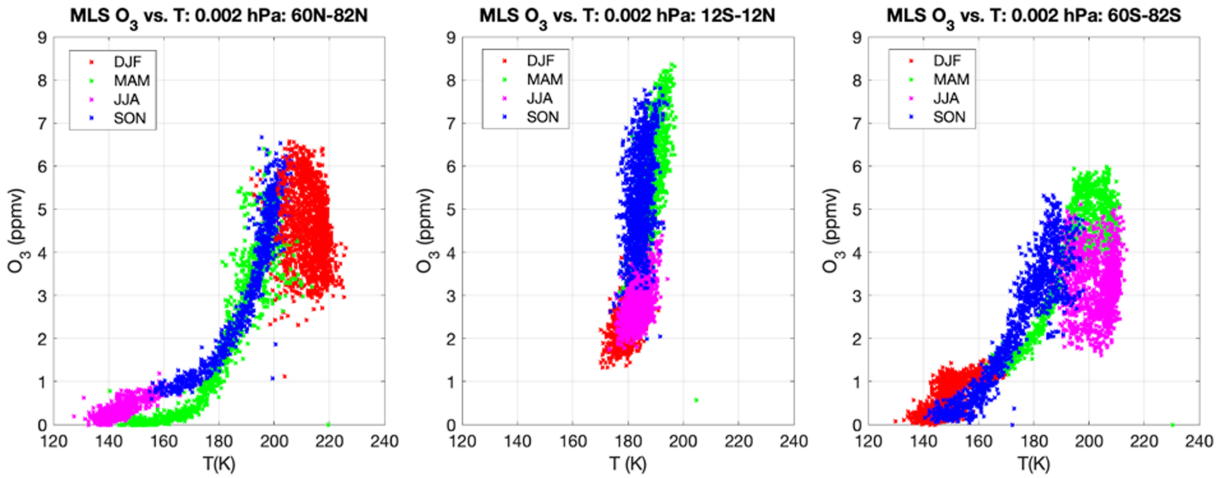

Figure 10. Mixing ratio correlation between MLS daily nighttime ozone (upper) and nighttime temperature (lower) during 2004–2017 at 0.002 hPa for northern high latitude (60°N–82°N) (left), tropics (12°S–12°N) (middle), and southern high latitude (60°S–82°S) (right). Red, green, magenta, and blue dots denote data during the months of DJF, MAM, JJA, and SON, respectively.

The ascending motions transport low amounts of ozone in the lower mesosphere to the upper mesosphere in the summer pole. Therefore, the positive ozone-temperature correlation near the mesopause is indicative of dynamically induced variations.

The negative correlation in the northern high-latitude winter, which mostly come from SSWs associated with polar mesospheric cooling, may indicate a period of time when the UMLT ozone is under chemical control, as suggested by Tweedy et al. (2013). Their model simulation shows that during SSWs the mesospheric upwelling induces mesospheric cooling, which is consistent with the idea of elevating the chemically controlled region to a higher altitude. The lack of negative correlation in the southern high-latitude winter implies a much weaker mesospheric upwelling without SSW.

4.2. Roles of Atomic Oxygen [O] and Eddy Diffusion

Since [(R5)] is the major source for atomic oxygen and CO in the UMLT, the eddy diffusion variation is expected to modulate both of their concentrations, as suggested in Garcia and Solomon (1985). As seen in the SME [O] observations (Thomas, 1990) and in the SCHIAMACHY observations (Kaufmann et al., 2014), the SABER daily mean [O] values also exhibit a SAO in the tropical upper mesosphere (Smith et al., 2010). The equinoctial maxima at this height are related to the SAO variation in k_{zz}. Because nighttime [O_3] in the UMLT is proportional to [O], its SAO is a manifestation of the SAO from [O], and the root cause is from the k_{zz} modulation.

In the UMLT, k_{zz} can be strongly modulated by the diurnal tide in the tropics. The diurnal tidal amplitude and k_{zz} are anticorrelated (Geller et al., 1997), and small-scale gravity waves are the major contributor to k_{zz} variations (e.g., Weinstock, 1984). Turbulence and mixing induced by breaking gravity waves are converted to k_{zz} in model parameterization schemes. Using model simulation experiments, Meyer (1999) and Akmaev (2001) found that larger k_{zz} values lead to weaker diurnal tide amplitudes in the UMLT region.

The observed tropical enhancement in nighttime [O_3] and [CO] at 0.002 hPa during equinox months is likely due to the weakened k_{zz} in the presence of strong diurnal tides. As shown in Figures S1 and S2, larger diurnal amplitudes occur in the equinox months in MLS upper mesospheric CO and temperature observations, implying a suppressed k_{zz} in the tropics. The SABER data reveal a similar seasonal variation in [O] (Smith et al., 2010). In fact, both [O] and [CO] exhibit a similar tidal pattern in latitude-height plot of day-night differences, suggesting that the diurnal tide may perturb these species systematically by modulating k_{zz} on an hourly basis.

Furthermore, because of their long lifetime in the UMLT, [CO] and [O] at 0.003–0.005 hPa are more abundant at winter high latitudes due to the mean meridional circulation and downward transport in the polar

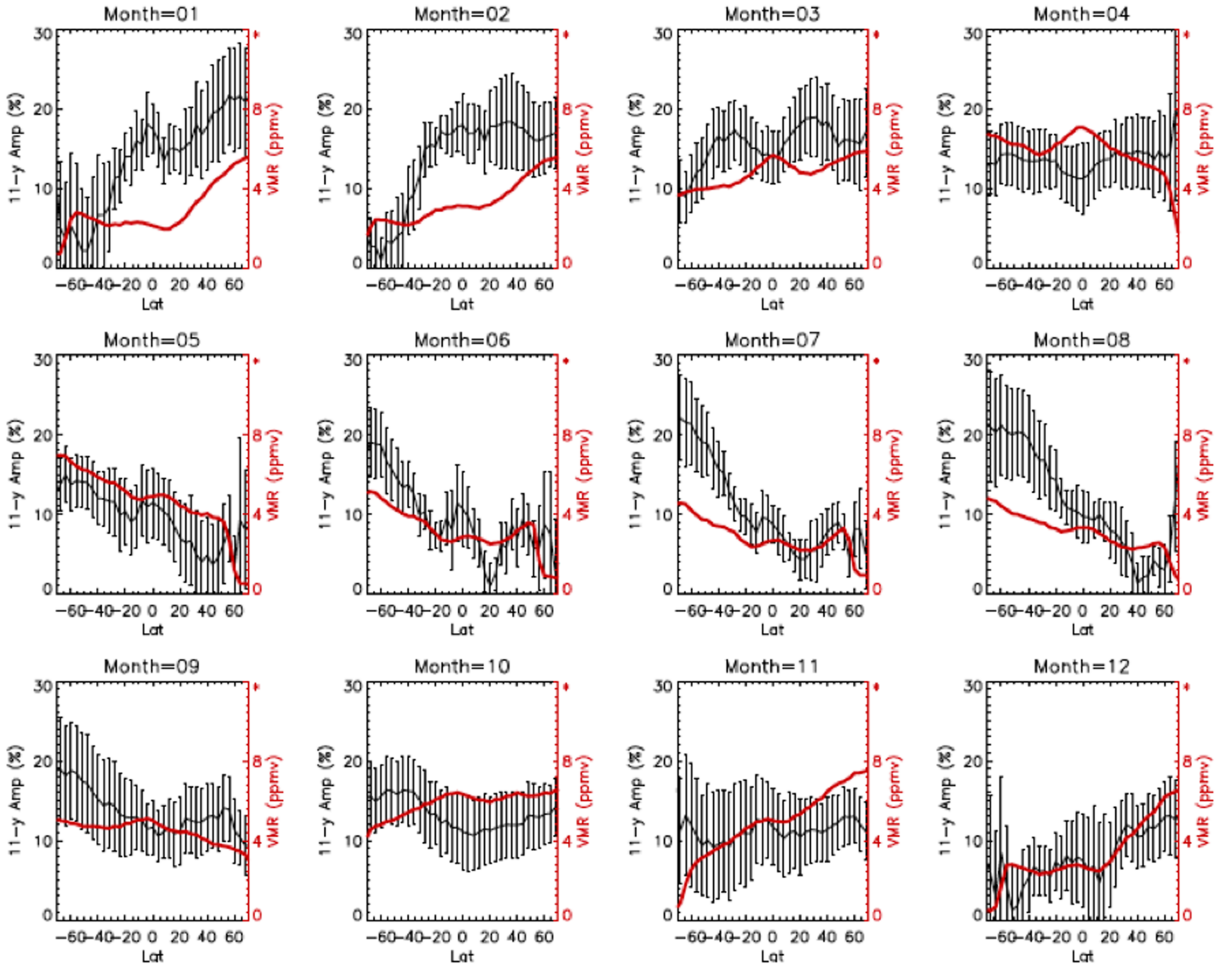

Figure 11. The amplitude of 11-year variation of nighttime O_3 at 0.002 hPa (in percentage) with standard deviation as a function of latitude. Overlaid red curves are mean O_3 VMR values (in ppmv).

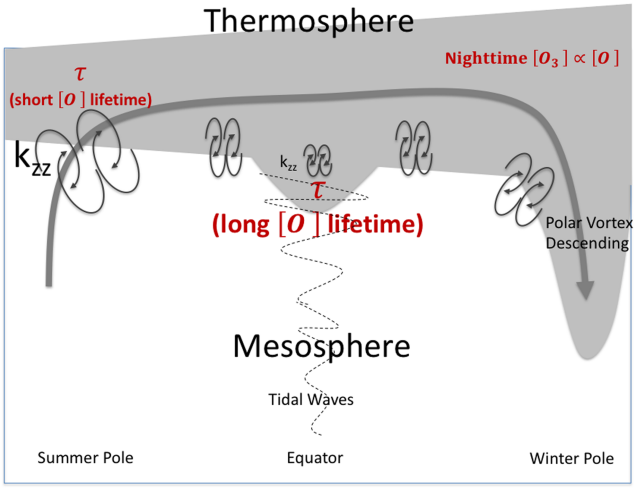

Figure 12. An illustration of vertical transport and eddy diffusion of $[O_3]$ and [O] in the middle atmosphere in relation to atomic oxygen, where k_{zz} and τ denote eddy diffusion coefficient and lifetime of atomic oxygen, respectively.

winter. This background transport in the upper mesosphere creates a large latitudinal gradient from winter to summer. As expected from its linear relationship with [O], the nighttime $[O_3]$ would follow the similar pole-to-pole gradient as seen in [CO].

It becomes complicated to determine what processes (i.e., dynamical vs. chemical) contribute mostly to the observed ozone 11-year variation, despite the clear in-phase correlation with the solar cycle. Salinas et al. (2018) showed that k_{zz} may have an 11-year variation, which can in turn modulate the [O] and [CO] concentrations and subsequently nighttime $[O_3]$ in the UMLT. If the solar cycle variation of nighttime $[O_3]$ were dominated by chemical processes, one would expect its 11-year amplitude to be proportional to its background mean. To help for this evaluation, Figure 11 compares the 11-year amplitude of nighttime ozone with its background at 0.002 hPa. Except for the months of April, October, and November, the ratio of solar cycle amplitude over the background nighttime ozone is not a constant across latitude. The dynamical contributions need to be considered to interpret the distribution of nighttime ozone solar cycle variations, as discussed in the previous section.

5. Conclusions

Our analyses of MLS nighttime ozone in the upper mesosphere at 0.002 hPa, coupled with past work on this topic, indicate that forcing from the 11-year solar cycle clearly affects interannual variations near the secondary ozone maximum, likely via direct photochemical processes as well as by indirect modulation of atomic oxygen transport. The O_3 distribution in the middle atmosphere is driven by vertical transport and eddy diffusion, as summarized by a simple diagram in Figure 12. Vertical transport inside the polar vortex brings anomalously large nighttime O_3 values from the lower thermosphere down to the upper mesosphere in high latitudes. Near the tropics, smaller k_{zz} and the increased lifetime of O_3 lead to small local increases in O_3 during equinox, as shown by the mean O_3 mixing ratios in Figure 11.

1. The MLS nighttime ozone seasonal climatology shows that MLS usefully samples the lower part of the secondary ozone maximum near 0.002 hPa, even though it does not cover the whole secondary maximum ozone layer in the UMLT. In general, there exist strong coherences in seasonal variations between MLS nighttime O_3 and CO in the UMLT. Both nighttime ozone and CO show a large annual cycle, with early winter (October/November in NH and April/May in SH) maxima and minima during local summer (DJF in NH and JJA in SH). They also show the SAO, as a secondary peak during local spring (February/March in NH and August/September in SH). In the tropics, the nighttime ozone seasonal variation shows the obvious SAO with two peaks during April and October, the April maximum being slightly larger than the later peak.
2. The positive correlation between nighttime ozone and solar UV irradiance at 240 nm indicates an apparent in-phase response of nighttime ozone to solar UV irradiance variation. The change of nighttime ozone over the solar cycle can be as high as 1.5 ppmv during winter. This amount corresponds to a 20–25% change in nighttime ozone change over the solar cycle.
3. MLS nighttime ozone and CO VMRs are highly correlated. Positive correlations between them are shown for each month. Similarities in solar cycle variations between nighttime ozone and carbon monoxide in the upper mesosphere suggest that there also exists a solar cycle in atomic oxygen [O] (which also has a long lifetime). While the distribution of [O] is challenging to measure, nighttime [O_3] could be viewed as a tracer for [O] at most latitudes.
4. The temperature dependence of nighttime ozone is not monotonously positive nor negative. The temperature-ozone correlations are generally positive, except at northern high latitudes in winter. Radiative heating due to ozone may result in regional warming and a positive correlation with temperature.

In this study, we analyzed 15 years of UV data at wavelengths near 240 nm. The solar cycle variation of solar spectral irradiance, including UV, is essential to elucidate wavelength-dependent terrestrial interactions with the Sun. In particular, reliable long-term UV data are a key element in characterizing the long-term changes of atmospheric constituents, that is, oxygen, ozone, and carbon monoxide, in both observational and modeling studies.

The Total and Spectral Solar Irradiance Sensor 1 was deployed with two instruments, Total Irradiance Monitor and Spectral Irradiance Monitor on the International Space Station in late 2017, to continue the total and spectral solar irradiance observations (200–2,400 nm). Absolutely calibrated satellite measurements of spectral solar irradiance are vital to be used as model inputs, since most of the climate models largely depend so far on the modeled solar spectrum. The value of such long-term solar irradiance observations, along with the fundamental middle atmosphere measurements cannot be overemphasized for the successful assessment of Earth's climate change in relation to solar forcing.

Acknowledgments
We thank two anonymous reviewers for valuable comments and suggestions which greatly helped to improve the manuscript. We thank J. Yue and M. Mlynczak for discussions on SABER, N. Livesey and L. Froidevaux on MLS ozone data, and M. Snow and J. Harder on solar spectral irradiances. We also acknowledge the MLS (https://disc.gsfc.nasa.gov/datasets?page=1&keywords=AURA%20MLS) and SORCE (http://lasp.colorado.edu/lisird/data/mission_data) data. This work is supported by NASA's Sun-Climate research at Goddard Space Flight Center.

References

Akmaev, R. A. (2001). Simulation of large-scale dynamics in the mesosphere and lower thermosphere with the Doppler-spread parameterization of gravity waves: 2. Eddy mixing and the diurnal tide. *Journal of Geophysical Research*, *106*, 1205–1213.

Allen, M., Lunine, J. I., & Yung, Y. L. (1984). The vertical distribution of ozone in the mesosphere and lower thermosphere. *Journal of Geophysical Research*, *89*, 4841–4872.

Andersson, M. E., Verronen, P. T., Rodger, C. J., & Seppälä, A. (2014). Missing driver in the Sun-Earth connection from energetic electron precipitation impacts mesospheric ozone. *Nature Communications*, *5*, 5197. https://doi.org/10.1038/ncomms6197

Aquila, V., Swartz, W. H., Waugh, D. W., Colarco, P. R., Pawson, S., Polvani, L. M., & Stolarski, R. S. (2016). Isolating the roles of different forcing agents in global stratospheric temperature changes using model integrations with incrementally added single forcings. *Journal of Geophysical Research: Atmospheres*, *121*, 8067–8082. https://doi.org/10.1002/2015JD023841

Ball, W. T., Rozanov, E., Alsing, J. A., Marsh, D. R., Tummon, F., Mortlock, D. J., et al. (2019). The upper stratospheric solar cycle ozone response. *Geophysical Research Letters*, *46*(3), 1831–1841. https://doi.org/10.1029/2018GL081501

Beig, G., Fadnavis, S., Schmidt, H., & Brasseur, G. P. (2012). Inter-comparison of 11-year solar cycle response in mesospheric ozone and temperature obtained by HALOE satellite data and HAMMONIA model. *Journal of Geophysical Research*, *117*, D00P10. https://doi.org/10.1029/2011JD015697

Brasseur, G., & Solomon, S. (2005). *Aeronomy of the middle atmosphere*. Dordrecht: D. Reidel Publishing Company.

Chapman, S. (1930). Memoirs of the royal meteorological society. *A theory of upper-atmospheric ozone* (Vol. III). London: Edward Stanford. No. 26

Crooks, S. A., & Gray, L. J. (2005). Characterization of the 11-year solar signal using a multiple regression analysis of the ERA-40 dataset. *Journal of Climate*, *18*, 996–1015.

Dhomse, S. S., Chipperfield, M. P., Damadeo, R. P., Zawodny, J. M., Ball, W. T., Feng, W., et al. (2016). On the ambiguous nature of the 11 year solar cycle signal in upper stratospheric ozone. *Geophysical Research Letters*, *43*, 7241–7249. https://doi.org/10.1002/2016GL069958

Dikty, S., Schmidt, H., Weber, M., von Savigny, C., & Mlynczak, M. G. (2010). Daytime ozone and temperature variations in the mesosphere: A comparison between SABER observations and HAMMONIA model. *Atmospheric Chemistry and Physics*, *10*, 8331–8339. https://doi.org/10.5194/acp-10-8331-2010

Dunkerton, T. J. (1982). Theory of the mesopause semiannual oscillation. *Journal of the Atmospheric Sciences*, *39*, 2682–2690.

Froidevaux, L., Jiang, Y. B., Lambert, A., Livesey, N. J., Read, W. G., Waters, J. W., et al. (2008). Validation of aura microwave limb sounder stratospheric ozone measurements. *Journal of Geophysical Research*, *113*, D15S20. https://doi.org/10.1029/2007JD008771

Garcia, R. R., López-Puertas, M., Funke, B., Marsh, D. R., Kinnison, D. E., Smith, A. K., & González-Galindo, F. (2014). On the distribution of CO_2 and CO in the mesosphere and lower thermosphere. *Journal of Geophysical Research: Atmospheres*, *119*, 5700–5718. https://doi.org/10.1002/2013JD021208

Garcia, R. R., & Solomon, S. (1985). The effect of breaking gravity waves on the dynamics and chemical composition of the mesosphere and lower thermosphere. *Journal of Geophysical Research*, *90*, 3850–3868. https://doi.org/10.1029/JD090iD02p03850

Gattinger, R. L., Kyrölä, E., Boone, C. D., Evans, W. F. J., Walker, K. A., McDade, I. C., et al. (2013). The roles of vertical advection and eddy diffusion in the equatorial mesospheric semi-annual oscillation (MSAO). *Atmospheric Chemistry and Physics*, *13*, 7813–7824. https://doi.org/10.5194/acp-13-7813-2013

Geller, M. A., Khattatov, B. V., Yudin, V. A., & Hagan, M. E. (1997). Modeling the diurnal tide with dissipation derived from UARS/HRDI measurements. *Annales de Geophysique*, *15*, 1198–1204.

Gruzdev, A., Schmidt, H., & Brasseur, G. (2009). The effect of the solar rotational irradiance variation on the middle and upper atmosphere calculated by a three-dimensional chemistry-climate model. *Atmospheric Chemistry and Physics*, *9*(2), 595–614. https://doi.org/10.5194/acp-9-595-2009

Haigh, J. D., Winning, A. R., Toumi, R., & Harder, J. W. (2010). An influence of solar spectral variations on radiative forcing of climate. *Nature*, *467*, 696–699. https://doi.org/10.1038/nature09426

Hocke (2017). Response of the middle atmosphere to the geomagnetic storm of November 2004. *Journal of atmospheric and solar-terrestrial physics*, *154*, 86–91. https://doi.org/10.1016/j.jastp.2016.12.013

Holton, J. R. (1983). The influence of gravity wave breaking on the general circulation of the middle atmosphere. *Journal of the Atmospheric Sciences*, *40*, 2497–2507.

Hood, L. L. (1986). Coupled stratospheric ozone and temperature responses to short-term changes in solar ultraviolet flux: An analysis of NIMBUS 7 SBUV and SAMS data. *Journal of Geophysical Research*, *91*(D4), 5264–5276. https://doi.org/10.1029/JD091iD04p05264

Hood, L. L., Huang, Z., & Bougher, S. W. (1991). Mesospheric effects of solar ultraviolet variations: Further analysis of SME IR ozone and Nimbus 7 SAMS temperature data. *Journal of Geophysical Research*, *96*(D7), 12,989–13,002. https://doi.org/10.1029/91JD01177

Hood, L. L., & Zhou, S. (1998). Stratospheric effects of 27-day solar ultraviolet variations: An analysis of UARS MLS ozone and temperature data. *Journal of Geophysical Research*, *103*(D3), 3629–3638. https://doi.org/10.1029/97JD02849

Huang, F. T., Mayr, H. G., Russell, J. M., Mlynczak, M., & Reber, C. A. (2008). Ozone diurnal variations and mean profiles in the mesosphere, lower thermosphere, and stratosphere, based on measurements from SABER on TIMED. *Journal of Geophysical Research*, *113*, A04307. https://doi.org/10.1029/2007JA012739

Hubert, D., Lambert, J. -C., Verhoelst, T., Granville, J., Keppens, A., & co-authors (2016). Ground-based assessment of the bias and long-term stability of 14 limb and occultation ozone profile data records. *Atmospheric Measurement Techniques*, *9*, 2497–2534. https://doi.org/10.5194/amt-9-2497-2016

Jackman, C. H., Marsh, D. R., Vitt, F. M., Garcia, R. R., Fleming, E. L., Labow, G. J., et al. (2008). Short- and medium-term atmospheric constituent effects of very large solar proton events. *Atmospheric Chemistry and Physics*, *8*, 765–785.

Jackman, C. H., Marsh, D. R., Vitt, F. M., Roble, R. G., Randall, C. E., Bernath, P. F., et al. (2011). Northern Hemisphere atmospheric influence of the solar proton events and ground level enhancement in January 2005. *Atmospheric Chemistry and Physics*, *11*(13), 6153–6166. https://doi.org/10.5194/acp-11-6153-2011

Kaufmann, M., Zhu, Y., Ern, M., & Riese, M. (2014). Global distribution of atomic oxygen in the mesopause region as derived from SCIAMACHYO(1S) green line measurements. *Geophysical Research Letters*, *41*, 6274–6280. https://doi.org/10.1002/2014GL060574

Lee, J. N., Cahalan, R. F., & Wu, D. (2016). Solar rotational modulations of spectral irradiance and correlations with the variability of total solar irradiance. *Journal of Space Weather and Space Climate*, *6*, A33. https://doi.org/10.1051/swsc/2016028

Lee, J. N., Wu, D. L., Manney, G. L., Schwartz, M. J., Lambert, A., Livesey, N. J., et al. (2011). Aura microwave limb sounder observations of the polar middle atmosphere: Dynamics and transport of CO and H_2O. *Journal of Geophysical Research*, *116*, D05110. https://doi.org/10.1029/2010JD014608

Lee, J. N., Wu, D. L., & Ruzmaikin, A. (2013). Interannual variations of MLS carbon monoxide induced by solar cycle. *Journal of Atmospheric and Solar - Terrestrial Physics*, *102*, 99–104. https://doi.org/10.1016/j.jastp.2013.05.012

Lee, J. N., Wu, D. L., Ruzmaikin, A., & Fontenla, J. (2018). Solar cycle variations in mesospheric carbon monoxide. *Journal of Atmospheric and Solar - Terrestrial Physics*, *170*, 21–34. https://doi.org/10.1016/j.jastp.2018.02.001

Leovy, C. B. (1964). Simple models of thermally driven mesospheric circulations. *Journal of the Atmospheric Sciences*, *21*, 327–341.

Li, K.-F., Zhang, Q., Tung, K.-K., & Yung, Y. L. (2016). Revolving a long-standing model-observation discrepancy in stratospheric ozone response to solar cycle. *Earth and Space Science*, *3*, 431–440.

Livesey, N. J., Read, W. G., Wagner, P. A., Froidevaux, L., Lambert, A., Manney, G. L., ... & Wang, S.. (2017). Version 4.2x level 2 data quality and description document, Tech. Rep. JPL D-33509 Rev. C, Jet Propulsion Lab.

Marsh, D. R., Skinner, W. R., Marshall, A. R., Hays, P. B., Ortland, D. A., & Yee, J.-H. (2002). High resolution Doppler imager observations of ozone in the mesosphere and lower thermosphere. *Journal of Geophysical Research*, *107*(D19), 4390. https://doi.org/10.1029/2001JD001505

Maycock, A. C., Matthes, K., Tegtmeier, S., Schmidt, H., Thiéblemont, R., Hood, L., et al. (2018). The representation of solar cycle signals in stratospheric ozone—Part 2: Analysis of global models. *Atmospheric Chemistry and Physics*, *18*, 11323–11343. https://doi.org/10.5194/acp-18-11323-2018

Maycock, A. C., Matthes, K., Tegtmeier, S., Thiéblemont, R., & Hood, L. (2016). The representation of solar cycle signals in stratospheric ozone—Part 1: A comparison of recently updated satellite observations. *Atmospheric Chemistry and Physics*, *16*, 10021–10043. https://doi.org/10.5194/acp-16-10021-2016

McClintock, W. E., Rottman, G., & Woods, T. N. (2005). Solar-stellar irradiance comparison experiment II (SOLSTICE II): Instrument concept and design. *Solar Physics*, *230*(1-2), 225–258. https://doi.org/10.1007/s11207-005-7432-x

McClintock, W. E., Snow, M., & Woods, T. N. (2005). Solar-stellar irradiance comparison experiment II (SOLSTICE II): Pre-launch and on-orbit calibrations. *Solar Physics*, *230*(1-2), 259–294. https://doi.org/10.1007/s11207-005-1585-5

Merkel, A. W., Harder, J. W., Marsh, D. R., Smith, A. K., Fontenla, J. M., & Woods, T. N. (2011). The impact of solar spectral irradiance variability on middle atmospheric ozone. *Geophysical Research Letters*, *38*, L13802. https://doi.org/10.1029/2011GL047561

Meyer, C. K. (1999). Gravity wave interactions with the diurnal propagating tide. *Journal of Geophysical Research*, *104*, 4223–4239.

Minschwaner, K., Manney, G. L., Livesey, N. J., Pumphrey, H. C., Pickett, H. M., Froidevaux, L., et al. (2010). The photochemistry of carbon monoxide in the stratosphere and mesosphere evaluated from observations by the Microwave Limb Sounder on the Aura satellite. *Journal of Geophysical Research*, *115*, D13303. https://doi.org/10.1029/2009JD012654

Qian, L., Solomon, S. C., & Kane, T. J. (2009). Seasonal variation of thermospheric density and composition. *Journal of Geophysical Research*, *114*, A01312. https://doi.org/10.1029/2008JA013643

Ruzmaikin, A., Santee, M. L., Schwartz, M. J., Froidevaux, L., & Pickett, H. (2007). The 27-day variations in stratospheric ozone and temperature: New MLS data. *Geophysical Research Letters*, *34*, L02819. https://doi.org/10.1029/2006GL028419

Salinas, C. C. J. H., Chang, L. C., Liang, M.-C., Qian, L., Yue, J., Lee, J. N., et al. (2018). Solar cycle response of CO_2 over the austral winter mesosphere and lower thermosphere region. *Journal of Geophysical Research: Space Physics*, *123*(9), 7581–7597. https://doi.org/10.1029/2018JA025575

Smith, A. K., Harvey, V. L., Mlynczak, M. G., Funke, B., García-Comas, M., Hervig, M., et al. (2013). Satellite observations of ozone in the upper mesosphere. *Journal of Geophysical Research: Atmospheres*, *118*, 5803–5821. https://doi.org/10.1002/jgrd.50445

Smith, A. K., & Marsh, D. R. (2005). Processes that account for the ozone maximum at the mesopause. *Journal of Geophysical Research, Atmospheres*, *110*, D23305. https://doi.org/10.1029/2005JD006298

Smith, A. K., Marsh, D. R., Mlynczak, M. G., & Mast, J. C. (2010). Temporal variations of atomic oxygen in the upper mesosphere from SABER. *Journal of Geophysical Research*, *115*, D18309. https://doi.org/10.1029/2009JD013434

Snow, M., McClintock, W. E., Rottman, G., & Woods, T. N. (2005). Solar-stellar irradiance comparison experiment II (SOLSTICE II): Examination of the solar stellar comparison technique. *Solar Physics*, *230*(1-2), 295–324. https://doi.org/10.1007/s11207-005-8763-3

Solomon, S., Garcia, R. R., Olivero, J. J., Bevilacqua, R. M., Schwartz, P. R., Clancy, R. T., & Muhleman, D. O. (1985). Photochemistry and transport of carbon monoxide in the middle atmosphere. *Journal of the Atmospheric Sciences*, *42*, 1072–1083.

Soukharev, B. E., & Hood, L. L. (2006). Solar cycle variation of stratospheric ozone: Multiple regression analysis of long-term satellite data sets and comparisons with models. *Journal of Geophysical Research*, *111*, D20314. https://doi.org/10.1029/2006JD007107

Studer, S., Hocke, K., Schanz, A., Schmidt, H., & Kämpfer, N. (2014). A climatology of the diurnal variations in stratospheric and mesospheric ozone over Bern, Switzerland. *Atmospheric Chemistry and Physics*, *14*(12), 5905–5919. https://doi.org/10.5194/acp-14-5905-2014, 2014. 32671, 32676, 32677

Swartz, W. H., Stolarski, R. S., Oman, L. D., Fleming, E. L., & Jackman, C. H. (2012). Middle atmosphere response to different descriptions of the 11-yr solar cycle in spectral irradiance in a chemistry–climate model. *Atmospheric Chemistry and Physics*, *12*, 5937–5948. https://doi.org/10.5194/acp-12-5937-2012

Tang, C., Wu, B., Wei, Y., Qing, C., Dai, C., Li, J., & Wei, H. (2018). The responses of ozone density to solar activity in the mesopause region and the mutual relationship based on SABER measurements during 2002–2016. *Journal of Geophysical Research: Space Physics*, *123*, 3039–3049. https://doi.org/10.1002/2017JA025126

Thiéblemont, R., Bekki, S., Marchand, M., Bossay, S., Schmidt, H., Meftah, M., & Hauchecorne, A. (2018). Nighttime mesospheric/lower thermospheric tropical ozone response to the 27-day solar rotational cycle: ENVISAT-GOMOS satellite observations versus HAMMONIA idealized chemistry-climate model simulations. *Journal of Geophysical Research: Atmospheres*, *123*, 8883–8896. https://doi.org/10.1029/2017JD027789

Thomas, R. (1990). Atomic hydrogen and atomic oxygen density in the mesopause region: Global and seasonal variations deduced from Solar Mesosphere Explorer near-infrared emissions. *Journal of Geophysical Research*, *95*(d10), 16457. https://doi.org/10.1029/JD095iD10p16457

Turunen, E., Kero, A., Verronen, P. T., Miyoshi, Y., Oyama, S.-I., & Saito, S. (2016). Mesospheric ozone destruction by high-energy electron precipitation associated with pulsating aurora. *Journal of Geophysical Research: Atmospheres*, *121*, 11,852–11,861. https://doi.org/10.1002/2016JD025015

Tweedy, O. V., Limpasuvan, V., Orsolini, Y. J., Smith, A. K., Garcia, R. R., Kinnison, D., et al. (2013). Nighttime secondary ozone layer during major stratospheric sudden warmings in specified-dynamics WACCM. *Journal of Geophysical Research: Atmospheres*, *118*, 8346–8358. https://doi.org/10.1002/jgrd.50651

Weinstock, J. (1984). Gravity wave saturation and eddy diffusion in the middle atmosphere. *Journal of Atmospheric and Terrestrial Physics*, ISSN: 0021–9169, *46*, 11.

Zhu, Y., & Kaufmann, M. (2018). Atomic oxygen abundance retrieved from SCIAMACHY hydroxyl nightglow measurements. *Geophysical Research Letters*, *45*, 9314–9322.

Zhu, Y., Kaufmann, M., Ern, M., & Riese, M. (2015). Nighttime atomic oxygen in the mesopause region retrieved from SCIAMACHY O(^{1}S) green line measurements and its response to solar cycle variation. *Journal of Geophysical Research: Space Physics*, *120*, 9057–9073. https://doi.org/10.1002/2015JA021405

Supporting Information for

Solar cycle modulation of nighttime ozone near the mesopause as observed by MLS

Jae N. Lee[1,*] and Dong L. Wu[2]

1. Joint Center for Earth Systems Technology, University of Maryland, Baltimore County, Baltimore, MD
2. NASA Goddard Space Flight Center, Greenbelt, MD

Contents of this file

Figures A1 to A2

This supporting information provides detailed information on Day-Night differences of MLS temperature and CO.

Day-Night differences of MLS temperature and CO

Aura MLS sampling is fixed in local time throughout the entire mission with ascending orbits at 1:30 AM and descending orbits at 1:30 PM at the equator, and we classified the MLS observation into daytime and nighttime data as described in section 2.1. By differencing the daytime and nighttime zonal mean data, diurnal tidal oscillations will emerge as the first order phenomenon. Figure A1-A2 show the day-night differences of MLS temperature and CO as a function of latitude. The oscillatory features in the upper mesosphere are indicative of the migrating diurnal tide, which is dominated by the (1,1) propagating mode. In this mode, both temperature and density variables have a peak at the equator and reverse the modal oscillations in sign at the subtropical latitudes. The vertical oscillatory features are a manifestation of vertical propagation of the tide, from which the vertical wavelength of the tidal wave is ~30 km from temperature observations. Because the CO VMR decreases substantially with height, the oscillations below ~80 km is hardly observable. It is clearly evident that the tidal amplitudes are larger in the months near the equinoxes. The ideal solution of the (1,1) mode is symmetric about the equator, but seasonal variations of the background winds can distort the hemispheric symmetry of the tide.

Figure captions

Figure A1. Day-night differences of MLS monthly temperature from 2004-2019. Contour intervals are 3K.

Figure A2. Day-night differences of MLS monthly CO from 2004-2019. Contour intervals are 1 ppmv.